Combustion and Flame 162 (2015) 3946–3959

Contents lists available at ScienceDirect

Combustion and Flame

journal homepage: www.elsevier.com/locate/combustflame

Structure of $CH_4/O_2/Ar$ flames at elevated pressures studied by flame sampling molecular beam mass spectrometry and numerical simulation

A.M. Dmitriev[a,b], D.A. Knyazkov[a,b,*], T.A. Bolshova[a], A.G. Tereshchenko[a], A.A. Paletsky[a], A.G. Shmakov[a,b], O.P. Korobeinichev[a]

[a] Voevodsky Institute of Chemical Kinetics and Combustion, Institutskaya str. 3, Novosibirsk 630090, Russia
[b] Novosibirsk State University, Pirogova str. 2, Novosibirsk 630090, Russia

ARTICLE INFO

Article history:
Received 29 March 2015
Revised 24 July 2015
Accepted 24 July 2015
Available online 11 August 2015

Keywords:
Methane combustion
Elevated pressure
Molecular beam mass spectrometry
Chemical kinetic modeling
Premixed flame

ABSTRACT

Experimental data are reported on the structure of laminar premixed methane/oxygen/argon flames stabilized over a flat burner at 1, 3, and 5 atm with different equivalence ratios ϕ (0.8–1.2). Mole fraction profiles of the reactants (CH_4, O_2), major stable products (CO_2, H_2O, H_2, CO) and intermediates such as H, OH, CH_3 radicals, as well as ethylene and acetylene, were measured by molecular-beam mass spectrometry. The temperature profiles in the flames were measured by thermocouples in the presence of a sampling probe to take into account the flame cooling effect due to the probe. The structures of stoichiometric flames at 1, 3 and 5 atm were compared to elucidate the effect of pressure on the mole fractions of the flame species. Fuel-lean ($\phi = 0.8$) and fuel-rich ($\phi = 1.2$) flames at 5 atm were also investigated in this work. All the experimental data were compared with the numerical simulations using the Premix code and three detailed chemical kinetic mechanisms for methane combustion available in the literature: the GRI-Mech 3.0, AramcoMech 1.3 and USC Mech II. The absolute mole fractions of CH_4, O_2, H_2O, CO, CO_2, H_2, H, OH, CH_3 in the flames and their dependences on pressure were captured by both mechanisms reasonably well. An analysis of the reaction mechanisms was performed to gain insights into the kinetics of methane combustion in stoichiometric conditions in the range of pressures from 1 to 5 atm and to explain the observed pressure effects on peak mole fractions of flame radicals. The decrease of peak mole fractions of acetylene and ethylene with pressure increase, which was observed in the experiments, was not reproduced by the mechanisms. Both mechanisms predicted the increase in their peak mole fractions with pressure (in the range from 1 to 3 atm). The kinetic analysis indicated the need to revise the pressure-dependent chemistry of acetylene and ethylene formation in the mechanisms.

1. Introduction

Combustion of hydrocarbons and of alternative fuels will remain to be the key source of energy in the foreseeable future. In addition, over the recent years, the requirements for the maximum concentrations of air pollutants produced when using devices based on combustion processes for energy production have become more stringent. Therefore, in order to design effective combustion devices and to determine conditions which are optimal to ensure effective combustion, the effects of which would be safe for the environment, it is necessary to know the precise chemical kinetics mechanisms of combustion of hydrocarbon fuels. In the actual devices (furnaces, combustion chambers of engines, turbines, etc.), the operating pressure is usually much higher than the atmospheric pressure and ranges from 10 to 100 atm.

The influence of pressure on the combustion chemistry is known to be manifested in the fact that, first, concentrations of species increase as the pressure rises, which leads to the growth of reaction rates and, second, the rate constants of many reactions depend on pressure (in accordance with the fall-off behavior). Currently, most chemical kinetics mechanisms for combustion of various hydrocarbons have been tested on experimental data obtained under laboratory conditions (species mole fractions in premixed flames and reactors, laminar flame speeds, ignition delay times in shock tubes, etc.) at much lower pressures. In particular, the data on the mole fractions of flame intermediates in burner-stabilized premixed flames, which are of prime importance for understanding combustion chemistry, have been mostly obtained only for low- and atmospheric-pressure conditions, which can be seen by the recent studies and reviews by different research groups [1–4]. It is evident that detailed reaction mechanisms, tested only for the atmospheric or low pressure

* Corresponding author. Fax.: +7 383 330 73 50.
E-mail address: knyazkov@kinetics.nsc.ru (D.A. Knyazkov).

http://dx.doi.org/10.1016/j.combustflame.2015.07.032
0010-2180/

conditions, cannot be securely applied to description of processes proceeding at higher pressures. To develop reliable reaction mechanisms, the available experimental database should be expanded to the area of higher pressures, and the mechanisms should be validated against this database. In this regard, recently more efforts have been taken to obtain data on different combustion characteristics (the laminar flame speed, the mole fraction profiles of intermediates and final combustion products, etc.) at high pressures, in order to test and further develop the available chemical kinetics models.

Methane is the basic component of natural gas and the intermediate product of combustion of heavy hydrocarbons. Any detailed chemical kinetics mechanism for combustion of heavy hydrocarbons includes methane oxidation reactions. Thus, the knowledge of the chemistry of methane combustion proceeding under conditions close to those in realistic combustion devices is of fundamental and practical importance.

The combustion and oxidation of methane under elevated pressures has been studied for quite a long time. In particular, the extensive experimental data on methane oxidation in flow reactors under high temperatures and pressures [5–10] formed the basis for the development of detailed chemical kinetic schemes for methane autoignition and oxidation.

A large number of studies have been focused on experimental and numerical simulation of the influence of pressure on the methane laminar flame speeds. For example, Goswami et al. [11] performed an exhaustive literature survey to study the numerous existing laminar burning velocity correlations for their pressure dependences. Using the heat flux method, they measured the laminar burning velocities of methane+air flames in the range of equivalence ratios from 0.8 to 1.4 for a pressure range between 1 and 5 atm. The data were found to be in good agreement with the measurements performed using the counterflow technique [12] and a constant-pressure combustion chamber [13], as well as with the calculations using GRI-Mech 3.0 [14] and USC Mech II [15] mechanisms. Rozenchan et al. [13], however, observed substantial deviations between the simulations using the GRI 3.0 mechanism and the experimental data for pressures above the range of 20–40 atm.

Serious attention has been recently paid to the processes of combustion of methane and other hydrocarbons at high pressures due to the problem of soot formation, see, e.g., [16] and references therein. In these studies, mostly optical methods are used to measure the soot volume fraction and temperature, see, e.g., [17]. Figura and Gomez [18] carried out GC–MS analysis of samples collected with a capillary probe in nitrogen-diluted ethylene–oxygen counterflow diffusion flames at various pressures up to 25 atm to measure concentrations of major species, aliphatics up to decane and aromatics up to indene, in order to address the effect of pressure on chemistry of formation of soot precursors.

Matynia et al. [19] measured concentration profiles of the OH radical, an important species in the combustion kinetics mechanisms, in CH_4/air and CH_4/CO_2/air laminar premixed counterflow flames, using the linear laser-induced fluorescence technique at different equivalence ratios (0.7–1.2) and pressures (1–7 atm). The OH mole fractions were found to be quantitatively well predicted by three different mechanisms, including GRI-Mech 3.0 at high pressures, while systematic overestimation by modeling was observed at atmospheric pressure.

Therefore, the experimental database needed to develop the reliable chemical kinetic mechanisms for hydrocarbons' combustion under conditions, which are close to realistic ones, should be completed with the data on the chemical speciation and temperature of flames at high pressures. The most informative method for obtaining data on the chemical kinetics mechanism of combustion is the molecular-beam mass spectrometry (MBMS) with electron impact ionization or tunable synchrotron vacuum ultraviolet photoionization. This method allows registration of not only stable species but also short-living intermediates in flames. The MBMS technique is widely used to study the flame structure of hydrocarbon fuels, including oxygen-containing fuels. However, these investigations were carried out only at low pressures (20–30 torr) [1], and at 1 atm, see, e.g. [2]. Only Paletskii et al. [20] used the method to measure the mole fraction of hydrogen, oxygen and water in the flat burner-stabilized H_2/O_2/Ar flame, at the pressure of 10 atm. To investigate the pressure effects on combustion chemistry, Zhou et al. [21] developed a combustion apparatus, combined with vacuum ultraviolet photoionization mass spectrometer, to study laminar premixed flames, and reported preliminary results obtained for premixed C_2H_4/O_2/Ar flames at pressures of 30, 150, and 760 torr. The authors believe the apparatus to be helpful in gaining insight into pressure-dependent combustion chemistry; however, this seems to be true only for pressures which are not higher than atmospheric.

In this study, the MBMS technique has been applied to measure the mole fraction profiles of different species in burner-stabilized premixed methane/oxygen/argon flames at the pressures of 1, 3 and 5 atm. The present work is focused on the measurement of the mole fraction profiles of H, OH and CH_3 radicals, which are key flame species, and also acetylene and ethylene, which are major flame intermediates playing an important role in formation of soot precursors. The objective of the study was to elucidate how the increase in pressure affects the species mole fractions in fuel-lean, stoichiometric and fuel-rich methane flames. In the present paper, the experimental results are compared with simulations obtained using the Premix code from the CHEMKIN package [22] and three detailed chemical kinetic mechanisms: the GRI-Mech 3.0 [14], the USC Mech II [15], and the recently updated AramcoMech 1.3 [23] mechanism. Reaction mechanisms are known to reproduce most of the experimental data in the best possible way for the near-stoichiometric conditions; however, in fuel-lean and fuel-rich flames the predictions are often not nearly so good. This motivated us to perform the measurements of the species mole fraction profiles in methane flames with different equivalence ratios, namely, 0.8, 1.0 and 1.2, at 5 atm, in order to check the chemical kinetic mechanisms' capability for predicting changes in the flame structure upon variation of fuel/oxidizer ratio under elevated-pressure conditions.

2. Experimental details

The flames of methane/oxygen/argon mixtures studied in this work were stabilized at the pressures of 1, 3 and 5 atm on home-made flat flame burners. Depending on the pressure range, the flames were stabilized on two different burners. Figure 1 shows a schematic of the high-pressure part of the experimental setup. The surface of the burner used for stabilizing the flames at 3 and 5 atm was a porous matrix made by pressing aluminum particles (~0.1 mm in diameter). Thus, the diameter of the pores through which the fresh mixture passed was not more than 0.1 mm. The matrix was 4 mm thick. The matrix was pressed into a base copper tube with an inner diameter of 6 mm. This diameter determined the size of the matrix, i.e. the diameter of the burner. The base copper tube was wrapped with another copper tube of smaller diameter, through which thermostated water was supplied. The good thermal contact between the base copper tube and the water supplying tube of the burner was ensured by soldering. The water temperature was maintained at 333 K. The burner was placed in a high-pressure brass housing, which was equipped with a micrometer screw mechanism and with inlets for connecting water and unburnt mixture supply. The screw mechanism allowed us to move the burner in a vertical direction relative to the housing. The copper tubes in which water and the fresh gas mixture were supplied to the burner were coiled inside the housing, so as not to allow, as the burner was moved relative to the housing, their excessive bend or breakage.

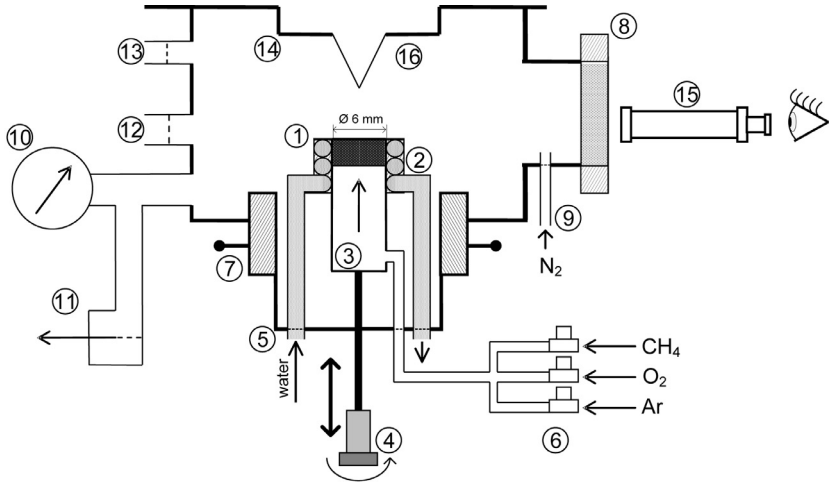

1- porous matrix
2- tube with circulating thermostated water
3- base tube
4- micrometer screw mechanism
5- brass enclosure
6- mass-flow controllers for unburnt gases supply
7- threaded connector
8- window for optical access
9 - inlet for pressurizing nitrogen supply
10- pressure gauge
11- exhaust line with pressure regulating valve
12- safety valve
13- thermocouple wires duct
14- sampling probe flange
15- cathetometer
16 – sampling probe

Fig. 1. Schematic of the high-pressure part of the experimental setup.

The brass housing, in which the burner was fixed, was attached tightly to the bottom of a stainless steel high-pressure chamber with an easily detachable threaded connector. The high-pressure chamber and the brass housing coupled together were designed to operate at the pressures of up to 10 atm. The chamber was equipped with a lateral flange for a window, which provided optical access for operator view. The nitrogen for pressurizing the chamber was supplied through the inlet in this flange to prevent condensation of water on the window and therefore to provide its transparence during the experiment. The chamber pressure was regulated by a diaphragm pressure regulator on the exhaust line, maintaining the set-point pressure within 1%. The chamber was equipped with a safety valve to ensure prompt gas evacuation in case of unexpected pressure surge and a gauge for pressure control. The chamber was also rigged with a manually operated three-coordinate mechanism for holding the thermocouple to measure the flame temperature. This mechanism allowed the operator to adjust precisely the thermocouple position relative to the probe tip.

The top flange of the high-pressure chamber was connected to the sampling probe flange of the molecular beam mass spectrometric setup. The MBMS setup has been described in detail in our previous works, in which we reported our experimental data obtained at atmospheric pressure in a variety of flames [2,24,25]. Briefly, the setup was a three-stage pumping system with vertical introduction of a molecular beam to the ion source of a quadrupole mass spectrometer with soft ionization by electron impact. The setup also included a quartz probe, a skimmer and a collimator. The second pumping stage (between skimmer and collimator) was equipped with a modulator of the molecular beam. The use of the beam modulator allowed us to discriminate the beam signal from the signal of background species and therefore to eliminate possible dependence of the signal on the background pressure in the ionization area.

In contrast to the experiments at atmospheric pressure, in which we used a quartz probe with an orifice of 80 microns in diameter and the opening angle of 40°, in this work, at pressures of 3 and 5 atm we used a sampling probe with the same opening angle and the orifice of 40 microns. The wall near the probe tip was 80 micron thick, and, getting closer to the base of the probe, it increased gradually and at the probe base the wall was 2 mm thick. The quartz cone, the geometry of which was described above, could withstand the pressure difference of atleast 10 atm. The height of the sampling probe, as measured from the base to the tip, was 18 mm. The mass flow rate through this sampling nozzle at the pressure of 5 atm was only 20% higher than through sampling nozzle with 80 micron orifice at a pressure of 1 atm (in our previous experimental conditions at atmospheric pressure). Due to the high pumping rate of the first-stage of the MBMS setup (between the sampling nozzle and skimmer), which was provided by the diffusion pump with evacuating capacity of 1100 l/s, the increase in the gas flow rate through the probe, indicated above, did not result in the increase of pressure in the ionization chamber and did not affect the quality of the molecular beam and thus the operation of the entire MBMS system. The pressure in the first stage (between sampling probe and skimmer), second stage (between skimmer and collimator), and third stage (ionization chamber) was $\sim 8.0 \cdot 10^{-4}$ torr, $4.0 \cdot 10^{-5}$ torr, and $1.0 \cdot 10^{-7}$ torr, respectively.

To perform the measurements at atmospheric pressure the flame was stabilized on a flat burner, which has been used in our previous studies [2]. The burner surface represented a perforated brass disc (diameter of holes 0.5 mm, hole separation 0.7 mm) 16 mm in diameter placed in a brass housing with a cooling jacket. The burner was filled with 3 mm diameter stainless steel balls to provide a uniform flow speed at the burner surface and to thoroughly heat the flow. The cooling jacket was thermostated by water at 333 K. The burner could be moved with the help of a micrometer screw mechanism in vertical direction. This mechanism as well as that one used for moving the high-pressure burner ensured the positioning of the burner relative to the sampling probe within the uncertainty of 10 microns. The thermocouple technique was also used to measure the temperature profile of the atmospheric pressure flame. The location of the thermocouple and the burner relative to the probe tip during the experiments at 1, 3 and 5 atm was controlled using a cathetometer.

The compositions of the fresh mixtures and their flow rates through the burner were selected on the following grounds. First, the flame temperature had to be lower than the melting point of quartz, the material used to make the probe. Second, the linear velocity of the fresh gas mixture at the burner exit had to be, on the one hand, not too high and not to exceed the flame burning velocity to ensure

Table 1
Molar composition, total flow rate (SLM: standard liters at 273 K per minute) and linear velocity (v) at the burner surface (at 333 K) of fresh mixtures and calculated (using GRI-Mech 3.0) laminar burning velocity (S_L) of the flames studied. The ratio v/S_L is also provided.

Flame	Eq. ratio, φ	P, atm	Mole fractions			Total flow rate, SLM	v, cm/s	S_L, cm/s	v/S_L
			CH_4	O_2	Ar				
Fuel-lean	0.8	5	0.0714	0.1786	0.75	1.24	17.8	35.8	0.497
Stoichiometric	1	1	0.0833	0.1667	0.75	2.74	27.9	68.69	0.400
	1	3	0.0833	0.1667	0.75	1.24	29.9	50.59	0.591
	1	5	0.0833	0.1667	0.75	1.24	17.9	42.28	0.423
Fuel-rich	1.2	5	0.0937	0.1563	0.75	1.24	17.8	34.55	0.515

stability of the flame on the burner and its flat front, and on the other hand, not too low. When the flow rate of the fresh mixture was too low, the flame clung to the burner surface very closely, which resulted in intense heat transfer to the burner. As at high pressures we used a small-diameter burner, at too low flow rates of the fresh mixture, the heat losses from the flame to the burner were so high that even the introducing the probe into the flame resulted in its extinction.

In choosing the flame conditions for the high-pressure experiments, we also noted that, when thermostated water of room temperature was supplied to the burner, the flame was unstable at the periphery. It turned out to be related to the following fact. Water formed during combustion, diffusing towards to the cold burner, condensed on it and, coming to the porous matrix at the burner periphery, boiled, perturbing the flame. We were able to solve the problem by raising the temperature of the thermostated water to 60 °C (333 K).

Making preliminary calculations of the flame speed and the maximum flame temperatures allowed us to select the most appropriate conditions for the experiment. The calculations were performed using the PREMIX code from the CHEMKIN II collection of codes [22] and the detailed chemical kinetic mechanism GRI-Mech 3.0. Altogether, 5 flames were investigated in this study. The composition and the total flow rate of the fresh gas mixtures investigated in this work are given in Table 1. This table also lists the linear velocities of the fresh mixtures at the burner surface (v), the adiabatic flame burning velocities (S_L) calculated using the GRI-Mech 3.0 mechanism. It was found empirically by visual observations that stable and flat flames were obtained when the ratio v/S_L was within the range from 0.4 to 0.6. Three stoichiometric flames of similar molar composition at the pressures of 1, 3 and 5 atm were investigated, in order to ascertain the impact of pressure on the profiles of the mole fractions of the flame species. In addition, two flames with different equivalence ratios (fuel-rich and fuel-lean) at the pressure of 5 atm were investigated. These data were required to check the ability of the combustion mechanisms to reproduce changes in the composition of intermediate and final combustion products in the flame, when the equivalence ratio changed under elevated-pressure conditions. The fresh mixtures of all the flames studied contained argon as a diluent, its mole fraction was the same in all the mixtures and equal to 0.75.

To account for the cooling effect of the probe on the flame, the temperature profiles in all the flames were measured, using a Pt-(Pt + 10% Rh) thermocouple located ~0.05 mm from the tip of the sampling probe in high-pressure flames and 0.2 mm from the probe tip in atmospheric-pressure flame. The thermocouple was welded from wires 0.02 mm in diameter, covered with a thin layer of SiO_2 to prevent catalytic effects on its surface. The resulting thermocouple had a diameter of 0.03 mm. The temperature values measured by the thermocouple were corrected for radiation heat losses as described elsewhere [26]. The measurements of the temperature profiles were repeated in each flame at least 4–5 times. The maximum spread in the measured values of the temperature was up to ±40 K. Therefore, this spread was considered as the temperature measurement uncertainty. Meanwhile, we are aware of the fact that the actual uncertainty of temperature measurements in the flame zone can be greater for the flames stabilized at 3 and 5 atm than for atmospheric-pressure flame due to greater temperature gradients.

Species mole fractions in both high-pressure and atmospheric-pressure flames as functions of height above burner (HAB) were measured, using a procedure described in detail in our previous works [2,24]. Thus, it is described below only briefly. For each species analyzed, individual electron energies were selected in order to obtain a sufficiently high signal-to-noise ratio and not to allow interferences caused by fragmentation of other species. The energies of ionizing electrons for most of the species were the same as those used earlier [2]. All the species measured in this work are listed in the Table 2. Also given in this table are their ionization energies, the energies of ionizing electrons used in this work and the calibration method applied. The cathetometer, which was used for the HAB control allowed us to determine it with the accuracy of ±10 μm.

The mole fractions of the reactants (CH_4, O_2), CO and stable intermediates (acetylene and ethylene) were determined using the calibration coefficients (relative to argon) derived from direct calibration experiments with gas mixtures of known composition. These

Table 2
Species measured in the flames.

m/z	Species	Species name	Ionization energy (eV)	Energy of ionizing electrons (eV)	Calibration method, comments
1	H	Hydrogen atom	13.6	16.2	RICS vs H_2 and post-flame partial equillibrium (see text)
2	H_2	Molecular hydrogen	15.43	16.65	H-element balance
15	CH_3	Methyl	9.84	12.3	RICS vs CH_4
16	CH_4	Methane	12.71	14.35	Direct
17	OH	Hydroxyl	13.02	16.2	RICS vs H_2O and post-flame partial equillibrium (see text)
18	H_2O	Water	12.62	15.4	O-element balance
26	C_2H_2	Acetylene	11.41	12.3	Direct
28	CO	Carbon monoxide	14.01	15.4	Direct
28	C_2H_4	Ethylene	10.53	12.3	Direct
32	O_2	Oxygen	12.07	14.35	Direct
40	Ar	Argon	15.76	16.3	Direct
44	CO_2	Carbon dioxide	13.80	15.4	C-element balance

mixtures were preliminarily heated to 470 K, to prevent clustering of argon before formation of the molecular beam in the sampling probe. It is noteworthy that the calibration coefficients for these species did not depend on the pressure (at least within the range from 1 to 5 atm). This indicates that the molecular beam is not affected by the pressure increase and therefore demonstrates reasonableness of our experimental observations described in the section below. The mole fraction of the major products (CO_2, H_2, H_2O) in the post-flame zone and the calibration coefficients for them were evaluated, using the material balance equations for C, O and H elements.

Calibration coefficients for H, OH and CH_3 radicals were determined by applying a relative ionization cross-section (RICS) method described by Cool et al. [27] and used in our previous work [2]. This method is described below only briefly. The calibration coefficient (S) links the signal intensity (I) with the mole fraction (X) for each species at a given temperature and pressure by a simple relation: $I = SX$. S is proportional to $\sigma(E)$, the ionization cross-section at electron energy E. Thus, the unknown calibration coefficient for an intermediate species is related to the known calibration coefficient for the nearest stable species by the following expression: $S_i = S_S \cdot [\sigma_i(E_i)/\sigma_S(E_S)]$, where index i corresponds to intermediate species, and index S corresponds to the nearest species with the known calibration coefficient. The electron ionization cross sections at a given electron energy were calculated using the NIST Electron Impact Cross Section Database [28].

The calibration coefficients for H and OH were also derived using an alternative method based on partial equilibrium by three "fast" reactions in the post-flame zone of the flames: $H_2 + OH \leftrightarrow H_2O + H$, $H_2 + O \leftrightarrow H + OH$, and $O_2 + H \leftrightarrow OH + O$, as done previously [24,25,29]. A good agreement between the calibration coefficients obtained with these two methods for H an OH was achieved.

The uncertainty of determining absolute mole fractions of the flame reactants and major products including intermediates (CO, CO_2, H_2O, H_2, C_2H_2, C_2H_4) was estimated to be ±15% of the maximum mole fraction values. Absolute mole fractions of H, OH and CH_3 radicals were determined to within a factor of about 2. This uncertainty factor is contributed by two error factors: the uncertainty in calibration coefficient of a particular radical and the error of measurement of its mass peak intensity. The uncertainty in the calibration coefficients determined using the RICS method was estimated to be about 50%, which is a combination of two factors: the ionization cross section error and the uncertainty in the calibration coefficient of a related nearest species. The measurement errors of mass peak intensities were mainly statistical and were reduced in the experiments to a minimum by increasing (within reasonable limits) the measurement time and the number of measurements of signal intensity for every mass peak. The resulting uncertainty of determining the mass peak signal intensity depends on many factors (the background signal, the species mole fraction in the flame, the setup sensitivity to a particular species, etc.) and is different for various mass peaks, but for most species measured, this uncertainty was not higher than 20%. Although the overall uncertainty of determination of the radicals' absolute mole fractions was quite high, their relative change with pressure was measured more accurate. This uncertainty was estimated to be basically determined by the measurement error of the corresponding mass peaks.

After all the calibrations were done, the resulting mole fractions of the species listed in Table 2 were normalized for each height above the burner to the sum of the mole fractions of all the species. Therefore, we get the species mole fractions, the sum of which for each HAB is equal to unity.

Insertion of a sampling probe into a flame disturbs the flame structure. However, there are too many factors to be taken into account to develop a universal recipe on how to correct the MBMS data for probe perturbations. The recent numerical studies [30] of sampling probe effects on the structure of flat burner-stabilized flames have demonstrated that three-dimensional CFD simulations, coupled with detailed chemical kinetics simulations, could be an effective tool in enhancing the interpretability of MBMS data. This numerical approach could also undoubtedly be helpful to interpret the experimental data obtained in this work under elevated pressure conditions; however, the computational cost for such a kind of simulations is relatively high. Therefore, at this point we used a widely accepted method to correct the experimental profiles for gas-dynamic probe perturbations: shifting them towards the burner by several probe orifice diameters. All the mole fraction profiles of a selected flame were shifted by the same distance. This distance was chosen for a flame so that the lowest HAB where the maximum mole fraction of water is achieved was the same as that one where the maximum temperature is reached. In particular, in our flame conditions the shift was 0.3, 0.02, and 0.06 mm for the flames at 1, 3, and 5 atm, respectively.

3. Modeling

The mole fraction profiles of the flame species were simulated, using the PREMIX code from the CHEMKIN II collection of codes. Three detailed chemical kinetic mechanisms were employed for modeling in this work: GRI-Mech 3.0 [14], USC Mech II [15] and AramcoMech 1.3 [23]. The thermodynamic and transport properties provided with each mechanism by the authors were used. The calculations were performed with the measured temperature profiles as input data using the TGIV keyword.

The GRI-Mech 3.0 mechanism [14], containing 53 species involved in 325 reversible reactions, is a mechanism widely employed in the literature for methane and natural gas combustion. As already stated in the Introduction section, it provided a good fit to the experimental data obtained at elevated pressures on laminar burning velocity of methane [11] and on OH mole fraction in counterflow methane flames [19].

USC Mech II [15] represents a $H_2/CO/C_1$–C_4 kinetic model, containing 111 species and 784 reactions, developed for prediction of a wide variety of combustion scenarios. It incorporates the thermodynamic, kinetic, and species transport data relevant to high-temperature oxidation of hydrogen, carbon monoxide, and C_1–C_4 hydrocarbons.

The AramcoMech 1.3 is a detailed reaction mechanism developed recently by the Combustion Chemistry Centre in NUI Galway. This mechanism, containing 253 species involved in 1542 reactions, characterizes the kinetic and thermochemical properties of a large number of C1-C3 based hydrocarbon and oxygenated fuels over a wide range of experimental conditions [31].

To explain the observed pressure effects on the structure of stoichiometric flames in the range 1–5 atm and to trace the origins of discrepancies between predicted and measured flame's structures, an analysis of the reaction pathways was performed. This analysis was performed in terms of the contributions (in percents) of the integrated rate of each individual reaction to the total integrated rate of consumption of the selected species in the entire flame. An integrated reaction rate (mol/cm^3) was calculated in the same way as was done in [32]:

$$\omega_i = \int_0^\infty \omega'_i dt = \int_0^\infty \frac{\omega'_i}{v} dx$$

where ω'_i is local rate of ith reaction, mol/(cm^3 s), v is local gas velocity (cm/s), x is distance from the burner (integration is carried out over the entire flame zone). To calculate the total integrated rate of consumption of a selected species, the summation was performed over all possible reactions associated with consumption of the very species.

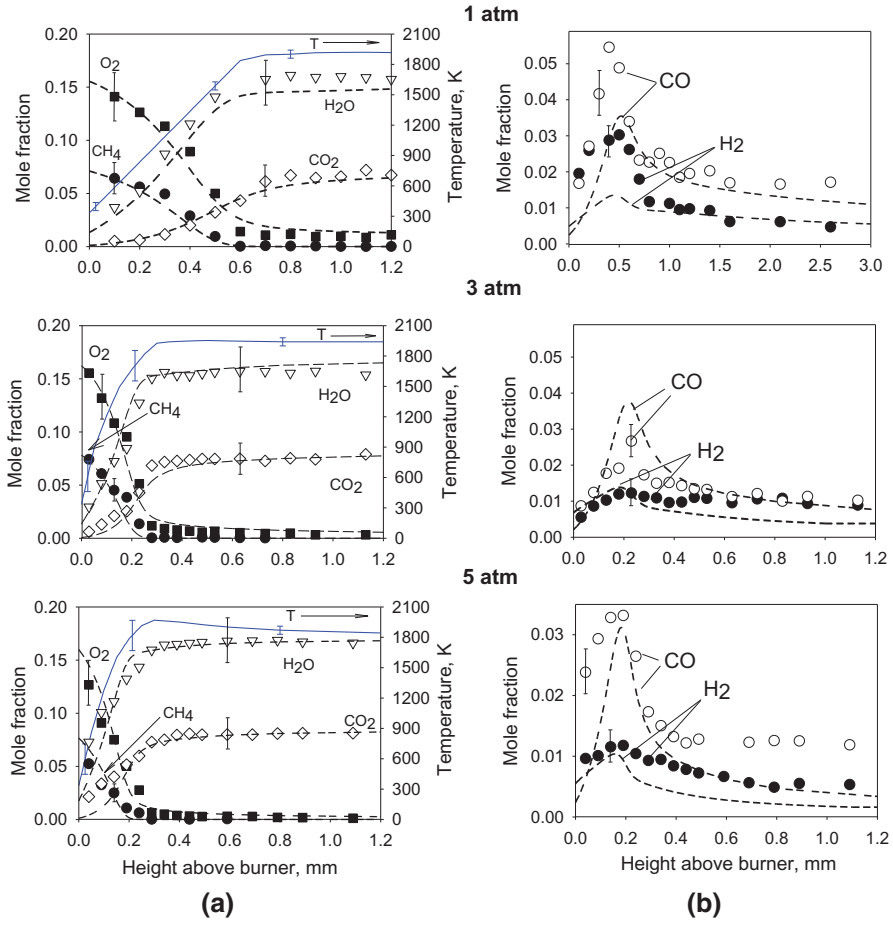

Fig. 2. Mole fraction profiles of major species and temperature profiles in stoichiometric ($\phi = 1.0$) $CH_4/O_2/Ar$ flames at different pressures. Symbols: experiment; dashed lines: modeling with GRI-Mech 3.0 (modeling with USC Mech II and AramcoMech 1.3 is not shown); solid lines: measured temperature profiles.

4. Results and discussion

The results of the experiments and calculations obtained in this work are shown in this section as follows. First, the experimental and numerical results obtained for the stoichiometric methane flames at different pressures (1, 3 and 5 atm) are presented. In Sections 4.1, 4.2 and 4.3, respectively, the pressure effects on major stable flame species, main flame radicals and the main C_1–C_2 intermediates in stoichiometric conditions are discussed and explained on the basis of the kinetic analysis. Then, in Section 4.4 the measured and predicted structures of fuel-lean and fuel-rich flames at 5 atm are compared with those for stoichiometric flame. The performances and deficiencies of the kinetic mechanisms in predicting the changes of the species mole fractions in the flames upon the variation of the equivalence ratio under 5 atm are discussed.

4.1. Pressure effect on temperature and major flame species in stoichiometric conditions

Figure 2a and b show mole fraction profiles of major species (CH_4, O_2, CO_2, H_2O, CO, H_2) and temperature profiles in stoichiometric ($\phi = 1$) methane/oxygen/argon flames at 1, 3 and 5 atm. In order not to overload the diagrams, CO and H_2 mole fraction profiles are plotted separately (Fig. 2b). In these figures, experimental data are compared with the results of numerical simulation. The calculations were performed using three kinetic mechanisms. For all the species indicated above all the mechanisms provided very close predictions of the mole fraction profiles; thus, in this figure we provided only the numerical results obtained using GRI-Mech 3.0.

As seen from Fig. 2a, the width of the flame zone largely decreases as the pressure increases from 1 to 3 atm, as expected: at the pressure of 1 atm, it is about 0.6 mm, while at 3 atm it is about 0.3 mm. It is interesting that under the selected experimental conditions, the pressure increase from 3 to 5 atm practically does not result in changing the width of the flame zone, although we had expected that it should decrease. This seems to be related to changes in the conditions of the heat exchange with the burner as the pressure rises, since in the experiments at 3 and 5 atm the mass flow through the burner was maintained to be constant, so the linear velocity of the fresh mixture near the burner surface at the pressure of 5 atm was lower than that at 3 atm (Table 1).

It is notable that maximum temperature gradients, as derived from the measured temperature profiles shown in Fig. 2a, comprise ~2500 K/mm for the 1 atm flame, and ~10,000 K/mm for the flames at 3 and 5 atm. Thus, the accuracy of the temperature measurements in the flame zone where these temperature gradients take place can be estimated as the thermocouple diameter (0.03 mm) multiplied by the value of the temperature gradient. For atmospheric-pressure flame this uncertainty is therefore about ±40 K (i.e. similar to that one declared above). For the flames at 3 and 5 atm, the experimental error limit is about ±150 K (at the heights above burner lower than ~0.2 mm). The error bars on the temperature profiles shown in Fig. 2a indicate the estimated experimental uncertainties at different heights above burner.

It is noteworthy that the maximum temperature of flame gradually grows as the pressure grows; however, this growth is

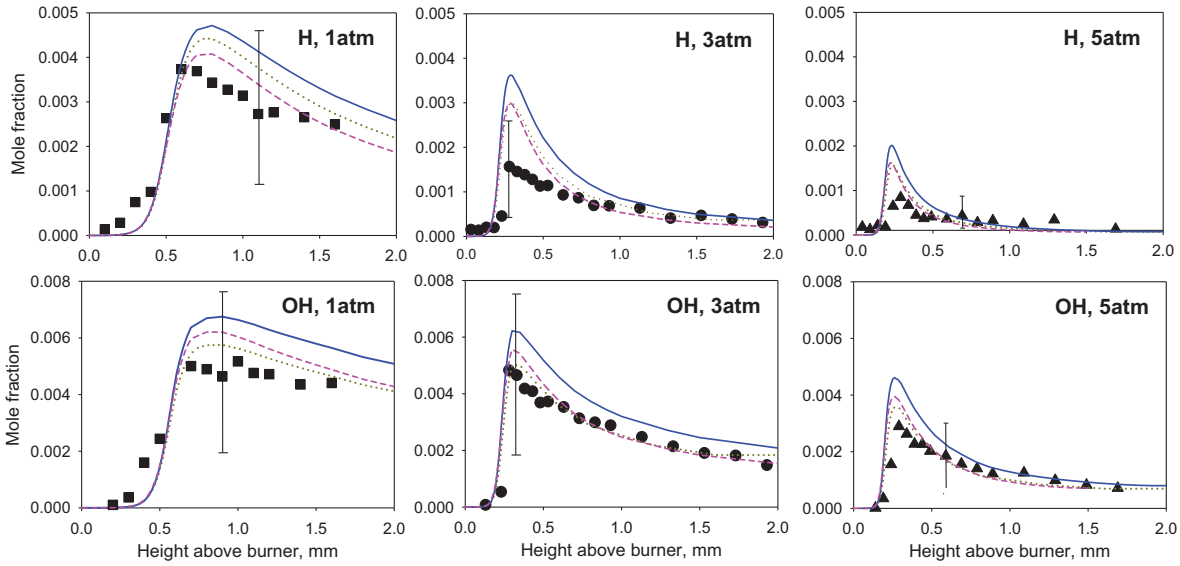

Fig. 3. Mole fraction profiles of H and OH radicals in stoichiometric CH_4/O_2/Ar flames at different pressures. Symbols: experimental data; lines: modeling. Solid line: AramcoMech 1.3; dashed line: USC Mech II; dotted line: GRI-Mech 3.0.

insignificant: the peak flame temperature at 1, 3 and 5 atm is 1917, 1940 and 1969 K, accordingly. These values are within the experimental error limit for thermocouple measurements. The fact that the maximum temperature in the flames is practically the same facilitates comparison of the reaction kinetics in these flames, because the temperature effect can be neglected. It should also be noted that at 5 atm the temperature profile has a characteristic peak (1969 K) at the distance of 0.3 mm from the burner surface, while at the distance of 1.2 mm from the burner surface the temperature value is 1843 K. This indicates that, as the pressure rises, the radiation losses ensure a greater temperature gradient in the post-flame zone (which was 140 K/mm in our experiments) than at atmospheric pressure, which is known to be about 100 K/cm [33] (depending on the burner diameter and the experimental conditions). As seen from Fig. 2, the mole fractions of the major flame products (CO_2, H_2O) in the post-flame zone do not decrease with the distance from the burner surface (at least up to HAB = 1.2 mm) at 5 atm, as well as at 3 atm, suggesting that there is no dilution of flame gases with surrounding nitrogen. Therefore, the decrease of temperature observed in the post-flame zone cannot be related to convective heat loss to the surrounding gas. Moreover, this observation, as well as the fact that the burner diameter is 20 times greater than the flame zone width (6 mm/0.3 mm = 20), also indicates the reasonableness of the choice of the burner diameter for our measurements at elevated pressures. For comparison, a typical ratio of the burner diameter to the flame zone width in our atmospheric-pressure measurements was 16–27, depending on the flame conditions [2,24,25].

As seen from Fig. 2a and b, the mole fraction profiles for CH_4, O_2, H_2O, CO_2, CO and H_2 obtained experimentally and by numerical simulation satisfactorily agree with one another. It should also be noted that the MBMS method with the sampling probe, the characteristics of which were described in the Experimental Details Section, ensures quite good spatial resolution, sufficient to trace the narrow flame zone, which is observed at 3 and 5 atm. As seen from Fig. 2, the increase of pressure to 5 atm actually does not result in the changes of the post-flame mole fractions of H_2O, CO_2, H_2, CO.

4.2. Pressure effect on H and OH radicals in stoichiometric conditions

Figure 3 shows the measured and calculated mole fraction profiles of H and OH, important flame radicals, in the stoichiometric flames at 1, 3 and 5 atm. The data shown in this figure for different pressures and for a particular species are represented in the same scale in order to provide visual demonstration of the pressure effect. One can see that, according to both experiments and computations, the pressure increase results in reduction of the peak mole fractions of H and OH radicals. This is in agreement with the observations of Matynia et al [19], who reported that OH concentration reduced in counterflow CH_4/air flame with pressure increase in the range from 0.1 to 0.7 MPa. Matynia and coworkers [19] explained this effect as associated with competition between the reactions of production and consumption of OH radicals, depending on the pressure. As seen from Fig. 3, all three mechanisms reproduce our experimental data well.

Concentration of the chain carriers (H, O and OH) in flames with a branched chain mechanism is known to be determined by the ratio of the branching and recombination reaction rates. Figure 4 shows the contributions (in percents) of the integrated rates of the reactions to the total integrated rate of production and consumption of H and OH radicals in stoichiometric methane flames at 1, 3 and 5 atm. This analysis was performed using AramcoMech 1.3 to explain the observed pressure effect on their mole fractions in the flame.

As can be seen from the diagrams shown, the pressure increase does lead to significant changes in the contribution of the main reactions of H and OH formation to the total integrated rate of H and OH production. The increase of pressure from 1 to 5 atm does not exert essential influence on the contribution of the rates of many reactions to the integrated consumption rate of H and OH. However, as can be seen from Fig. 4, as the pressure increases from 1 to 3 atm, the contribution of the recombination reaction $H+OH+M \leftrightarrow H_2O+M$ to consumption of H and OH radicals essentially increases (at the pressure of 1 atm, the contribution of this reaction is negligibly small) but changes little as the pressure rises from 3 to 5 atm.

It also follows from the diagrams shown, that, as the pressure increases from 1 to 3 atm, the contribution of the reaction $H+O2(+M) \leftrightarrow HO2(+M)$ to the integrated consumption rate of H occurs; while, as the pressure further rises to 5 atm, the contribution to the consumption of the OH radical is ensured by the reaction $HO_2+OH \leftrightarrow H_2O+O_2$. Therefore, the pressure dependence of mole fractions of key radicals in methane stoichiometric flames, and, hence, of the overall combustion kinetics, is largely determined by competition of $H + O_2(+M) \leftrightarrow HO_2(+M)$ and HO_2 reactions with radicals with the main branching reactions. Burke et al. [34,35] also pointed out this fact basing on their experimental data on

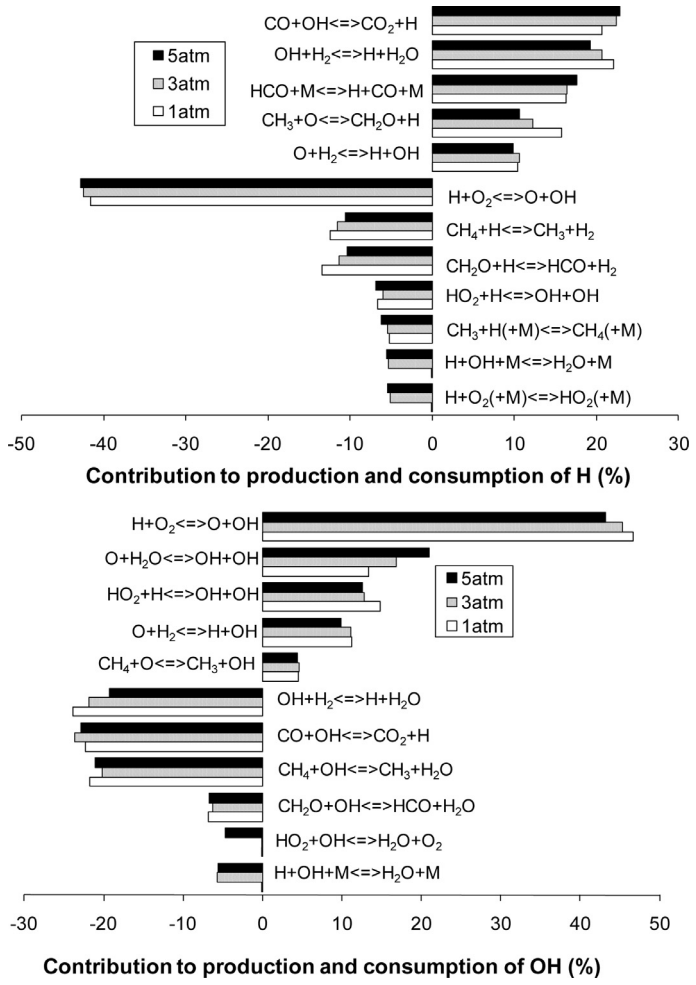

Fig. 4. Major contributions (in percents) of the integrated rates of the reactions to the total integrated rate of production and consumption of H (top) and OH (bottom) radicals in stoichiometric CH_4/O_2/Ar flames at 1, 3 and 5 atm.

Table 3
Experimental (H_2O_{exp}) and equilibrium (H_2O_{eq}) mole fractions of water and their ratio in stoichiometric flames at 1, 3 and 5 atm. Water equilibrium mole fractions were calculated for the corresponding temperatures measured in the post-flame zone ($T_{post\text{-}flame}$).

P, atm	$T_{post\text{-}flame}$, K	H_2O_{exp}	H_2O_{eq}	$H_2O_{exp}/H_2O_{eq} \times 100$, %
1	1908	0.16	0.1708	93.22
3	1940	0.16	0.1710	93.95
5	1843	0.17	0.1715	97.52

burning rates and reaction pathway analysis for lean and stoichiometric $H_2/CH_4/O_2$/diluent flames in pressure range from 1 to 25 atm.

Thus, the changes with pressure indicated above result in reducing the mole fractions of H and OH radicals in flame (Fig. 3) and bringing the system closer to thermodynamic equilibrium. To demonstrate it, in Table 3 we compared the values of the mole fraction of water (the main product of H and OH recombination), measured in the post-flame zone [H_2O_{exp}], with thermodynamic equilibrium values [H_2O_{eq}], calculated for the same temperature values which were measured in the post-flame zone. As can be seen from the table, the ratio [H_2O_{exp}]/[H_2O_{eq}] × 100% increases with pressure from ~93.2% (at 1 atm) to ~97.5% (at 5 atm).

When pressure rises from 1 to 5 atm, the measured peak mole fraction H reduces more than twice, while the peak mole fraction of OH decreases approximately 1.5 times (Fig. 3). We performed additional analysis of the AramcoMech 1.3 mechanism in order to explain why OH mole fraction reduces less than that of H as the pressure rises in our conditions, and we obtained the following result. Increase of pressure results in the increase of the rate of the trimolecular recombination reaction $H + O_2(+M) \leftrightarrow HO_2(+M)$. Comparison of the calculated peak mole fractions of the HO_2 radical in two flames (at 1 and 5 atm) has shown that, unlike H, OH, and O, mole fraction of HO_2 increases with pressure. In the flame at the pressure of 1 atm, the peak mole fraction of HO_2 is 1.26×10^{-4}, and in the flame at 5 atm it is 1.43×10^{-4}. In atmospheric-pressure flame, HO_2 is formed in the reactions $CH_2OH + O_2 \leftrightarrow CH_2O + HO_2$ and $HCO + O_2 \leftrightarrow CO + HO_2$. The rate of reaction $H + O_2(+M) \leftrightarrow HO_2(+M)$ increases with pressure. In the flame at 5 atm, its integrated rate is about half of the total integrated rate of HO_2 formation. The main pathway of HO_2 consumption is ensured by the reaction of recombination with the H radical, with two OH radicals formed: $HO_2 + H \leftrightarrow OH + OH$. The role of reaction $CH_3 + HO_2 \leftrightarrow CH_3O + OH$, which also results in the formation of OH radical, increases with pressure.

Thus, the processes described above contribute to the fact that the mole fraction of the OH radical in flame decreases with the pressure not so much as the mole fraction of the H radical. This, in its turn, leads to the increased role of reactions involving OM radical as the pressure rises.

4.3. Pressure effect on CH_3, C_2H_2 and C_2H_4 in stoichiometric conditions

The mole fraction profiles of another important flame radical, CH_3, and also of acetylene and ethylene, which are important C_2-intermediates responsible for formation of soot precursors, under stoichiometric conditions at different pressures are shown in Fig. 5. As can be seen, all three mechanisms yield very similar results for CH_3 mole fraction profiles at all pressures. The mechanisms overpredict the values of CH_3 mole fraction at all pressures, but nevertheless the data for CH_3 at 3 and 5 atm are predicted by the mechanisms much better than those at 1 atm (the experimental data for CH_3 at 1 atm are multiplied by 5 in the figure). The numerical predictions using GRI-Mech 3.0 for C_2H_2 and C_2H_4 mole fraction profiles differ significantly from those provided by USC Mech II and AramcoMech 1.3, which in turn are in close agreement. AramcoMech 1.3 and USC Mech II provide higher values of the mole fraction of these species than GRI-Mech 3.0 throughout the flame zone. It is interesting to note that USC Mech II and AramcoMech 1.3 accurately predict mole fraction profiles of C_2H_2 and C_2H_4 at atmospheric pressure, but overpredict mole fractions of these species at 3 and 5 atm, whereas the GRI-Mech 3.0 is more accurate in reproducing the experimental data for these species at 3 and 5 atm, but underpredicts their mole fractions at 1 atm.

For illustration, Fig. 6 demonstrates experimental and calculated peak mole fractions of CH_3, C_2H_2 and C_2H_4 as functions of pressure. As seen from the figure, all mechanisms predict a similar CH_3 peak mole fraction trend with pressure increase, which is in a good qualitative agreement with experimental observations. In the range from 1 to 3 atm, the measured peak mole fractions of C_2H_2 and C_2H_4 virtually do not change, and slightly decrease with increasing pressure to 5 atm. However, the mechanisms predict more than double growth of the peak mole fractions of C_2H_2 and C_2H_4 when pressure is increased from 1 to 3 atm, and practically unchanged peak mole fraction of C_2H_2 and C_2H_4 as the pressure is further increased to 5 atm (AramcoMech 1.3 and USC Mech II predict only slight reduction of C_2H_4 peak mole fraction with pressure increase from 3 to 5 atm). It is interesting to point out that Figura and Gomez [18] reported a nearly constant C_2H_2 peak mole fraction trend with pressure increase (in the range from 0.1 to 0.8 MPa) in ethylene–oxygen counterflow diffusion flames. By comparison, the experimental data obtained by Kailasanathan et al. [36] in an ethylene/air laminar jet diffusion flame at elevated pressures in the range 1-8 atm however showed that the peak mole fraction of C_2H_2 does not depend on pressure in the range

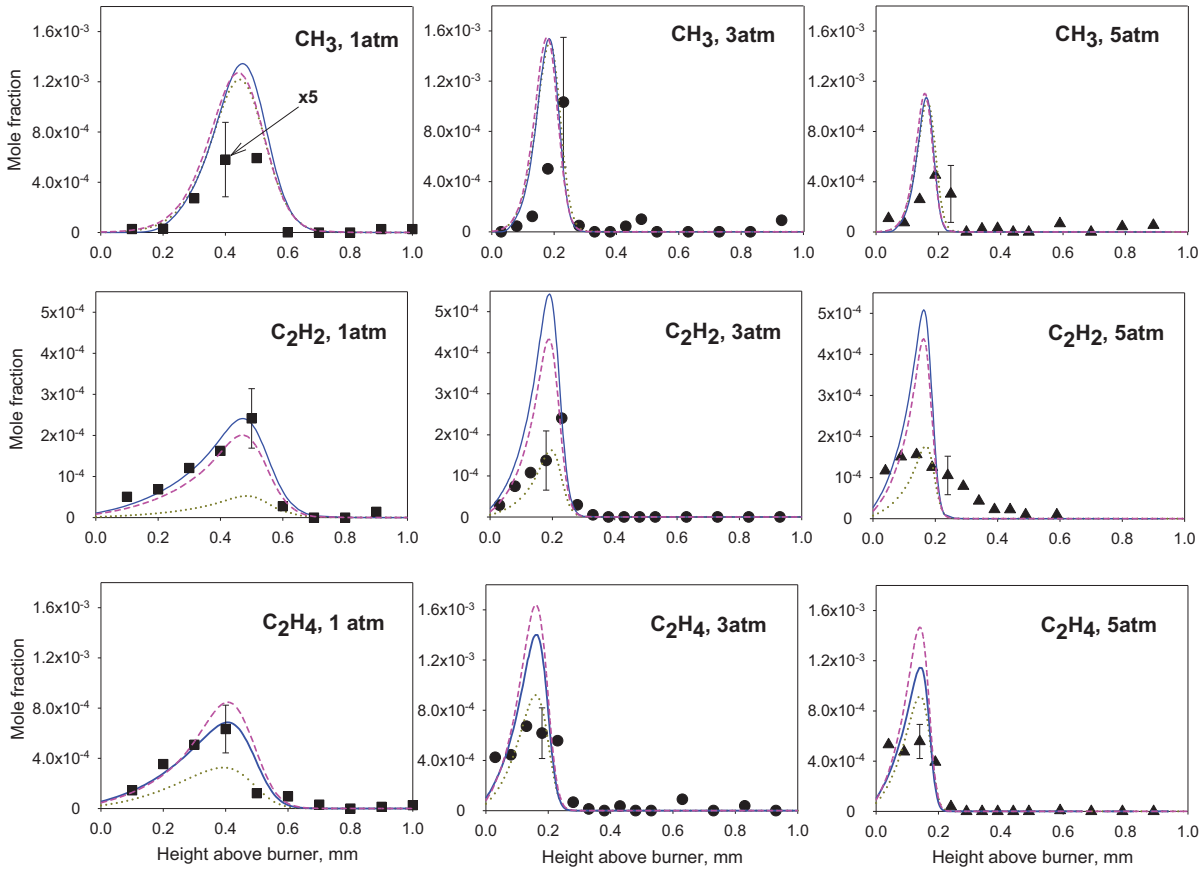

Fig. 5. Mole fraction profiles of methyl radical, acetylene and ethylene in stoichiometric $CH_4/O_2/Ar$ flames at different pressures. Symbols: experimental data; lines: modeling. Solid line: AramcoMech 1.3; dashed line: USC Mech II; dotted line: GRI-Mech 3.0.

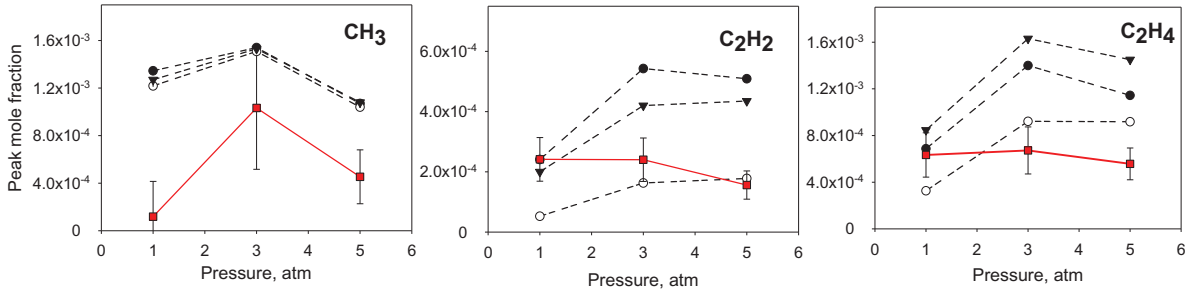

Fig. 6. Pressure dependences of maximum mole fractions of methyl radical, acetylene and ethylene. Squares and solid lines: experimental data. Symbols and dashed lines: modeling. Filled circles: AramcoMech 1.3; filled triangles: USC Mech II; open circles: GRI-Mech 3.0.

1–2 atm and reduces with further pressure increase. Therefore, our experimental results for C_2H_2 show a tendency which is close to that observed in [36].

As seen from Fig. 6, neither mechanism predicts adequately the pressure dependence of the peak mole fraction of C_2H_2 and C_2H_4. To ascertain the reasons of these divergences between the models and the experiment as well as to explain the effects of pressure on the flame species under stoichiometric conditions, an analysis of the chemical kinetic mechanisms was performed. Here, we confined ourselves to the analysis of GRI-Mech 3.0 and AramcoMech 1.3 only, because, as is seen above, USC Mech II provides very similar predictions and pressure tendencies to those given by AramcoMech 1.3. The diagrams of the main reaction fluxes for consumption of methane and its products, composed basing on the two mechanisms, are shown in Fig. 7, combining results for the flames at 1, 3 and 5 atm. The diagram corresponding to GRI-Mech 3.0 is at the top and that for AramcoMech 1.3 is at the bottom of the Fig. 7. Each branch in this figure is shown with the values, representing contributions (in percents) of the integrated rate of each individual reaction to the total integrated rate of consumption of the selected species in the entire flame (top values: 1 atm, values in the middle: 3 atm, bottom values: 5 atm).

The first thing to note in the diagrams shown in Fig. 7 is that, as the pressure changes, the major pathways of methane transformation into the final products remain to be unchanged in both mechanisms. Change of pressure affects only the contribution of a particular reaction to consumption of a selected flame species.

According to both mechanisms, fuel oxidation begins with reactions of CH_4 with OH, H and O radicals, with methyl radical formed. In this pathway, transformation of 99–100% parent fuel occurs; therefore the further process of oxidation is determined entirely by the possible ways of methyl radical consumption, which are somewhat different in the mechanisms used.

In accordance with GRI-Mech 3.0, there are several major pathways of CH_3 consumption. It should be first pointed out that one of

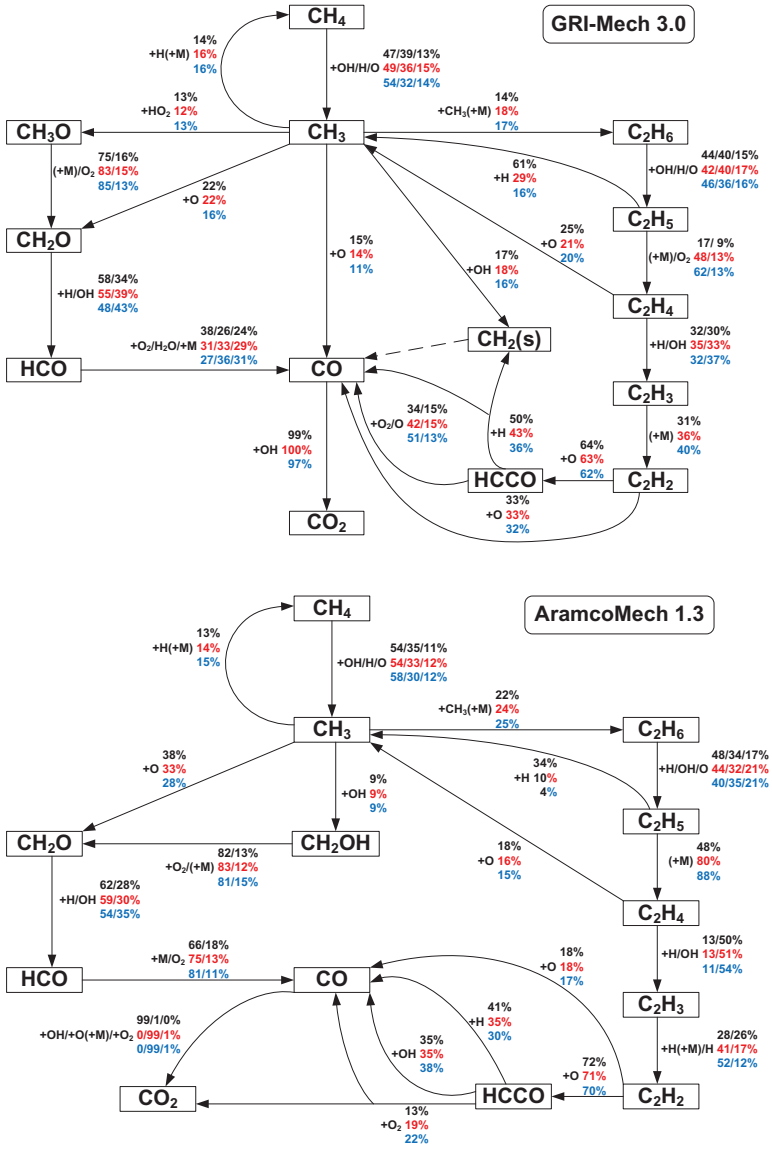

Fig. 7. Main reaction pathways of methane oxidation in stoichiometric $CH_4/O_2/Ar$ flame according to GRI-Mech 3.0 and AramcoMech 1.3 mechanisms. Contributions of the integrated rate of each individual reaction to the total integrated rate of consumption of the selected species are shown. Top values: 1 atm, values in the middle: 3 atm, bottom values: 5 atm.

them is the transformation pathway back into methane by a trimolecular reaction with atomic hydrogen $CH_3 + H\,(+M) \leftrightarrow CH_4\,(+M)$. Another pathway is provided by the reactions with direct formaldehyde formation $CH_3 + O \leftrightarrow CH_2O + H$ or through formation of the metoxy radical ($CH_3 + HO_2 \leftrightarrow CH_3O$), which turns into CH_2O by the following reactions:

$$CH_3O\,(+M) \leftrightarrow CH_2O + H\,(+M)$$

$$CH_3O + O_2 \leftrightarrow CH_2O + HO_2$$

Another pathway of methyl radical consumption is its reaction with the OM radical, with $CH_2(S)$ formed:

$$CH_3 + OH \leftrightarrow CH_2(S) + H_2O \qquad (R1)$$

This pathway further leads to formation of CO via the following chain of transformations $CH_2(S) \rightarrow CH_2 \rightarrow CH \rightarrow HCO \rightarrow CO$ (this chain is not shown in the schematic but is indicated by a dashed arrow from $CH_2(S)$ to CO). The reaction of CH_3 with the oxygen atom ensures a direct pathway of methyl transformation into CO:

$$CH_3 + O \leftrightarrow CO + H_2 + H. \qquad (R2)$$

Finally, the recombination reaction of two methyl radicals with a third body participating in it ensures another pathway of CH_3 consumption, the product of which is ethane:

$$2CH_3\,(+M) \leftrightarrow C_2H_6\,(+M). \qquad (R3)$$

It is interesting that in the AramcoMech 1.3 formation of formaldehyde from CH_3 proceeds also through two major pathways: direct (similarly as in GRI-Mech 3.0) and indirect, via formation of CH_2OH (but not CH_3O, as in GRI-Mech 3.0):

$$CH_3 + OH \leftrightarrow CH_2OH + H$$

$$CH_2OH + O_2 \leftrightarrow CH_2O + HO_2$$

$$CH_2OH(+M) \leftrightarrow CH_2O + H(+M)$$

Unlike GRI-Mech 3.0, the AramcoMech 1.3 mechanism does not include a direct pathway of CH_3 transformation into CO (R2), and the

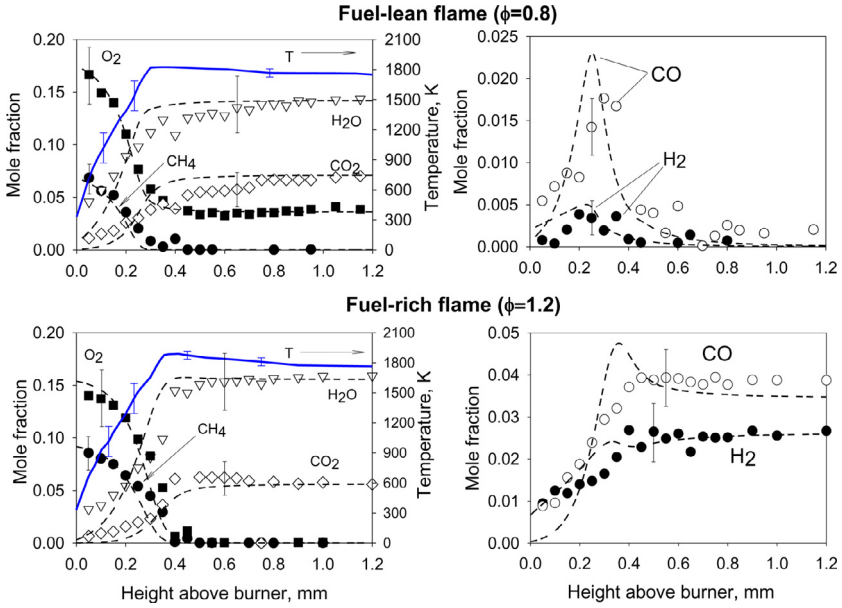

Fig. 8. Mole fraction profiles of major species and temperature profiles in fuel-lean ($\phi = 0.8$) and fuel-rich ($\phi = 1.2$) $CH_4/O_2/Ar$ flames at 5 atm. Symbols: experimental data; dashed lines: modeling with GRI-Mech 3.0 (modeling with AramcoMech 1.3 and USC Mech II is not shown); solid lines: measured temperature profiles.

reaction R1 plays a less significant role, therefore it is not shown in the bottom schematic in Fig. 7.

According to both mechanisms, formaldehyde converts eventually to CO through formyl (HCO) formation in the reactions with H and OH: $CH_2O + H \leftrightarrow HCO + H_2$ and $CH_2O + OH = HCO + H_2O$. Formyl transforms then to CO via bimolecular H abstraction reactions, two of which are similar in both mechanisms:

$$HCO + M \leftrightarrow CO + H + M$$

$$HCO + O_2 \leftrightarrow CO + HO_2$$

and the reaction $HCO + H_2O \leftrightarrow H + CO + H_2O$ is also considered only in the GRI-Mech 3.0.

Another branch of transformations of methyl radical into CO is represented by formation of C_2 hydrocarbons through the following chain: $CH_3 \rightarrow C_2H_6 \rightarrow C_2H_5 \rightarrow C_2H_4 \rightarrow C_2H_3 \rightarrow C_2H_2 \rightarrow HCCO \rightarrow CO$. This chain begins with formation of ethane (R3), which participates in reactions with H, O and OH radicals, with ethyl formation:

$$C_2H_6 + OH \leftrightarrow C_2H_5 + H_2O$$

$$C_2H_6 + H \leftrightarrow C_2H_5 + H_2$$

$$C_2H_6 + O \leftrightarrow C_2H_5 + OH$$

Decomposition of C_2H_5 occurs along two pathways: with formation of CH_3 by the reaction

$$C_2H_5 + H \leftrightarrow 2CH_3 \qquad (R4)$$

and with formation of C_2H_4 by the reaction

$$C_2H_5(+M) \leftrightarrow C_2H_4 + H(+M), \qquad (R5)$$

and, according to the GRI-Mech 3.0, also by the reaction

$$C_2H_5 + O_2 \leftrightarrow C_2H_4 + HO_2 \qquad (R6)$$

In both mechanisms, ethylene is consumed mainly through reactions with M and OM radicals, with the vinyl radical (C_2H_3) formed: $C_2H_4 + H \leftrightarrow C_2H_3 + H_2$, $C_2H_4 + OH \leftrightarrow C_2H_3 + H_2O$. Its reaction with atomic oxygen contributes to CH_3 and HCO formation: $C_2H_4 + O \leftrightarrow CH_3 + HCO$. The vinyl radical is the major source of acetylene in flame by the reactions:

$$C_2H_3 + H \leftrightarrow C_2H_2 + H_2$$

$$C_2H_3 + H(+M) \leftrightarrow C_2H_2 + H_2(+M)$$

Then acetylene in reactions with atomic oxygen gets oxidized to CO ($O + C_2H_2 \leftrightarrow CO + CH_2$) or to HCCO ($C_2H_2 + O \leftrightarrow H + HCCO$), which eventually also converts with CO formed in reactions with M and OM radicals, and with CO_2 and CO formed in the reaction $HCCO + O_2 \leftrightarrow CO + CO_2 + H$.

It is interesting to note that conversion of CO–CO_2 at atmospheric pressures in both mechanisms seems to occur exclusively by the reaction with hydroxyl $CO + OH \leftrightarrow CO_2 + H$. According to GRI-Mech 3.0, when pressure increases this reaction also remains to be dominant. However, in the AramcoMech 1.3 mechanism at the pressures of 3 and 5 atm, conversion of CO to CO_2 is determined by the trimolecular reaction with atomic oxygen: $CO + O(+M) \leftrightarrow CO_2(+M)$.

The above-described schemes of major reaction pathways of methane conversion at different pressures, obtained by analyzing two kinetic mechanisms, demonstrate the following regularity: as the pressure grows, the role of bimolecular reactions with the OM radical increases, whereas the role of the reactions with H radical, on the contrary, decreases or remains practically unchanged (see, for instance, the percentage values shown in the schemes in Fig. 7 for the following pathways: $CH_4 \rightarrow CH_3$, $CH_2O \rightarrow HCO$, $C_2H_4 \rightarrow C_2H_3$, $HCCO \rightarrow CO$). It seems that the increased role of reactions involving OH in the general scenario of methane oxidation is due to the change in the ratio between the mole fractions of the H and OH radicals in flame with pressure rise, which was discussed above in Section 4.2. However, the change in the contribution of these reactions due to the pressure growth generally does not exert essential influence on the major reaction pathways, as well as the role of reactions with participation of O radicals (see, for example, the pathways $C_2H_4 \rightarrow CH_3$, $C_2H_2 \rightarrow CO$, $C_2H_2 \rightarrow HCCO$, $CH_4 \rightarrow CH_3$). Apparently, this explains the fact that the mole fraction of CH_3, which is produced and consumed in the flames mainly due to reactions involving these radicals, has no definite tendency to increase or decrease with increasing pressure

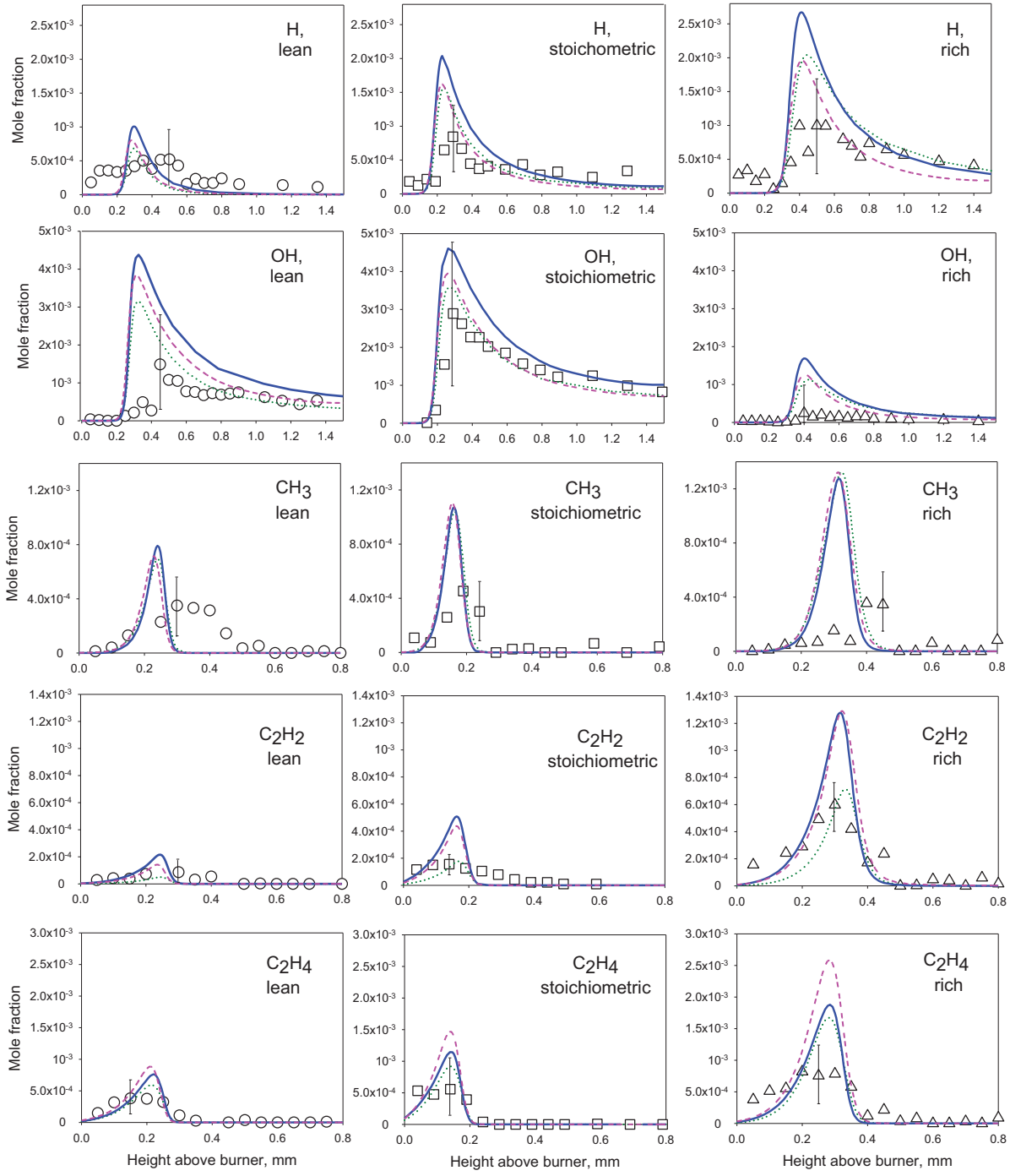

Fig. 9. Mole fraction profiles of flame radicals, acetylene and ethylene in fuel-lean ($\phi = 0.8$), stoichiometric ($\phi = 1.0$) and fuel-rich ($\phi = 1.2$) CH_4/O_2/Ar flames at 5 atm. Symbols: experimental data; lines: modeling. Solid line: AramcoMech 1.3; dashed line: USC Mech II; dotted line: GRI-Mech 3.0.

and every time depends on what channel plays a more important role under the given conditions.

As seen from Fig. 7, the increase of pressure most strongly affects the consumption pathways of the ethyl radical (reactions R4 and R5). First of all, this is determined by the dependence of the reaction rate constant of reaction R5 on pressure. Although the fall-off behavior of the rate constant of this reaction is given by the parameters, which are different in the mechanisms used, both these mechanisms predict a similar trend for the contribution of this reaction to the total rate of consumption of the ethyl radical with pressure increase. As the pressure rises, the contribution of this pathway to consumption of ethyl (with the formation of ethylene) increases; according to both mechanisms, the strongest growth of the rate of this reaction is observed when changing from 1 to 3 atm. Thus, the contribution of this reaction to the total ethyl consumption rate when changing from 1 to 3 atm increases from 48 to 80%, according to the AramcoMech 1.3, and from 17 to 48%, according to the GRI-Mech 3.0. As the pressure further increases to 5 atm, the increase of the contribution of this reaction is also observed; yet, it is not so essential (from 80 to 88% in AramcoMech 1.3 and from 48 to 62% in GRI-Mech 3.0), compared to that observed in the pressure range from 1 to 3 atm. The following two facts result from the increase of the contribution of reaction R5 to ethyl consumption: (1) contribution of reaction R4 to its consumption decreases as the pressure grows (from 61 to 16%,

according to the GRI-Mech 3.0, and from 34 to 4%, according to the AramcoMech 1.3) and (2) the rate of ethylene formation grows as the pressure rises. As it follows from the above, the peak mole fraction of ethylene (see Fig. 6) calculated with both mechanisms for the range of pressures from 1 to 3 atm essentially grows, while, as the pressure further grows to 5 atm, according to the GRI 3.0 mechanism, it remains approximately the same, and, according to AramcoMech 1.3, it decreases by about 20%. A similar pressure dependence is demonstrated by the peak mole fraction of acetylene (Fig. 6), calculated by both mechanisms, as the chemistry of conversion of acetylene and ethylene is closely connected (it can be seen from the schemes shown in Fig. 7).

However, our experimental observations, which, as already said, turned out to be close to the observations of other researchers, demonstrated a totally different behavior of the peak mole fractions of C_2H_4 and C_2H_2 (see Fig. 6) with pressure. This indicates that the pressure-dependent chemistry of acetylene and ethylene formation should be revised in the mechanisms, however, it is not the goal of the present research. Moreover, this underlines the importance of the third-body and fall-off reactions in the overall kinetics of methane combustion. Therefore, the kinetic models to be elaborated in the future for hydrocarbons combustion at high pressures should involve more such reactions.

4.4. The structure of fuel-lean and fuel-rich methane flames at 5 atm

Figure 8 shows the mole fraction profiles of reactants (CH_4 and O_2) and major products (H_2O, CO_2, CO and H_2) in fuel-lean ($\phi = 0.8$) and fuel-rich ($\phi = 1.2$) methane flames at 5 atm. In this figure, the temperature profiles measured in these flames are also represented. The measurements showed the maximum temperatures of these flames to be lower than that of stoichiometric flame at 5 atm (for comparison: 1820 K in the lean flame, 1969 K in the stoichiometric flame and 1885 K in the rich flame), indicating that the maximum heat release occurs under stoichiometric conditions, all other conditions being equal. The mechanisms ensured very close predictions of spatial variations of the mole fraction of these flame species over the burner, thus in this figure only the curves obtained by numerical simulation using GRI-Mech 3.0 are plotted. As can be seen, the calculations are in a good agreement with the experimental data. Increasing the equivalence ratio from 0.8 to 1.2 virtually does not influence the post-flame mole fractions of water and carbon dioxide; however, it results in increasing post-flame mole fractions of hydrogen and carbon monoxide and also leads to complete consumption of oxygen in the flame.

The mole fraction profiles of intermediates measured in fuel-lean ($\phi = 0.8$) and fuel-rich ($\phi = 1.2$) methane flames at 5 atm are compared in Fig. 9 with those measured in the stoichiometric flame and calculated by using the kinetic mechanisms. Both experiment and calculations generally show a similar trend of change of the species peak mole fractions as the equivalence ratio increases. As expected, increasing the fuel-to-oxidizer ratio in the fresh mixture results in the increase in the peak mole fraction of such species as H, C_2H_2, C_2H_4. According to the experimental observations, the methyl radical peak mole fraction remains nearly unchanged as the equivalence ratio increases, whereas both mechanisms predict its increase. All mechanisms predict nearly the same OH peak mole fraction in the lean and in the stoichiometric flame, although the experiment shows its increase, when the equivalence ratio increases from 0.8 to 1.0. These discrepancies may be due to the high experimental uncertainty with the absolute mole fraction values of the flame radicals. Both calculations and measurements show a reduction of the OH peak mole fraction when the equivalence ratio changes from 1.0 to 1.2. It is worth noting that all mechanisms provide similar predictions of the mole fraction profiles of CH_3 only. For other flame intermediates, as can be seen from Fig. 9, AramcoMech 1.3 and USC Mech II yield higher values of mole fractions through the whole flame zone than GRI-Mech 3.0 does, thus providing a worse fit to the experimental data.

Therefore, in general, all mechanisms tested predict adequately the effect of the equivalence ratio change on the peak mole fractions of intermediates and on the mole fractions of the major products in methane flame at 5 atm. The quantitative discrepancies observed between the predictions and measurements can serve as indications for the mechanism developers to refine the reaction rate constants and pathways responsible for production and consumption of the species discussed in this work. In particular, an attention should be paid to the reaction pathways of formation and consumption of acetylene and ethylene at different pressures and equivalence ratios.

5. Conclusions

In this work, the mole fraction profiles of the reactants, the major stable products and some intermediates including H, OH and CH_3 radicals, as well as ethylene and acetylene, were measured by a flame-sampling molecular-beam mass spectrometric technique in laminar premixed burner-stabilized $CH_4/O_2/Ar$ flames at different equivalence ratios ϕ (0.8–1.2) and pressures (1–5 atm). In total, 5 flames are investigated: 3 stoichiometric flames at 1, 3 and 5 atm, and 2 flames at 5 atm with ϕ equal to 0.8 and 1.2. The experimental data were compared with the results of numerical simulations using two detailed chemical kinetic mechanisms for methane combustion: GRI-Mech 3.0, USC Mech II and AramcoMech 1.3. The simulations were performed using the temperature profiles measured by thermocouples in the presence of the sampling probe to take into account the flame cooling effect by the probe. All three mechanisms, in general, adequately predicted absolute mole fractions of CH_4, O_2, H_2O, CO, CO_2, H_2, H, OH, CH_3 in the flames and their dependence on pressure. However, the decrease of peak mole fractions of acetylene and ethylene with pressure increase, which was observed in the experiments, was not reproduced by the mechanisms. The mechanisms predicted the increase in their peak mole fractions with pressure (in the range from 1 to 3 atm).

An analysis of the reaction mechanisms has been presented to gain insights into the kinetics of methane combustion under stoichiometric conditions in the range of pressures from 1 to 5 atm and to explain the observed pressure effects on peak mole fractions of flame radicals. It was found that under stoichiometric conditions, as the pressure rises, the peak mole fraction of M reduces more than the peak mole fraction of OM. As a result, the contributions to the overall process of methane transformation of the reactions involving OH instead of H increase with increasing pressure. The kinetic analysis showed that this could be related primarily to the reaction $H + O_2 (+M) \leftrightarrow HO_2 (+M)$, the contribution of which to H consumption increases with pressure. As a consequence, HO_2 production is enhanced with pressure contributing to the formation of OH via the reactions of HO_2 with H and CH_3 radicals. Based on the results of kinetic analysis, it was concluded that pressure-dependent chemistry of acetylene and ethylene formation should be revised in the mechanisms to provide adequate prediction of pressure influence on their mole fractions. The experimental data represented in this work can be used for testing and validation of many other chemical kinetic models for methane combustion, which were not mentioned here.

Acknowledgments

This work was supported by the Russian Foundation for Basic Research under grant No: 13-03-00823.

References

[1] N. Hansen, T.A. Cool, P.R. Westmoreland, K. Kohse-Höinghaus, Prog. Energy Combust. Sci 35 (2) (2009) 168–191.
[2] I.E. Gerasimov, D.A. Knyazkov, S.A. Yakimov, T.A. Bolshova, A.G. Shmakov, O.P. Korobeinichev, Combust. Flame 159 (2012) 1840–1850.
[3] F.N. Egolfopoulos, N. Hansen, Y. Ju, K. Kohse-Höinghaus, C.K. Law, F. Qi, Prog. Energy Combust. Sci. 43 (2014) 36–67.

[4] V. Dias, H.M. Katshiatshia, H. Jeanmart, Combust. Flame 161 (9) (2014) 2297–2304.
[5] T.B. Hunter, H. Wang, T.A. Litzinger, M. Frenklach, Combust. Flame 97 (2) (1994) 201–224.
[6] T.A. Ano, F.L. Dryer, Proc. Combust. Inst. 27 (1) (1998) 397–404.
[7] H. Schwarz, M. Geske, C. Franklin Goldsmith, R. Schlögl, R. Horn, Combust. Flame 161 (7) (2014) 1688–1700.
[8] C.L. Rasmussen, A.E. Rasmussen, P. Glarborg, Combust. Flame 154 (3) (2008) 529–545.
[9] T. Le Cong, P. Dagaut, Proc. Combust. Inst. 32 (1) (2009) 427–435.
[10] Z. Chen, X. Qin, Y. Ju, Z. Zhao, M. Chaos, F.L. Dryer, Proc. Combust. Inst. 31 (1) (2007) 1215–1222.
[11] M. Goswami, S.C.R. Derks, K. Coumans, W.J. Slikker, M.H. de Andrade Oliveira, R.J.M. Bastiaans, C.C.M. Luijten, L.P.H. de Goey, A.A. Konnov, Combust. Flame 160 (2013) 1627–1635.
[12] F.N. Egolfopoulos, P. Cho, C.K. Law, Combust. Flame 76 (1989) 375–391.
[13] G. Rozenchan, D.L. Zhu, C.K. Law, S.D. Tse, Proc. Combust. Inst. 29 (2002) 1461–1469.
[14] G.P. Smith, D.M. Golden, M. Frenklach, N.W., Moriarty, B. Eiteneer, M. Goldenberg, C.T. Bowman, R.K. Hanson, S. Song, W.C. Gardiner Jr., V.V. Lissianski, Z. Qin, GRI Mech 3.0, 1999, available at http://www.me.berkeley.edu/gri_mech/.
[15] H. Wang, X. You, A. Joshi, S.G. Davis, A. Laskin, F.N. Egolfopoulos, C.K. Law, High-temperature combustion reaction model of H2/CO/C1–C4 compounds, USC Mech II, 2007, available at http://ignis.usc.edu/USC_mech_II.htm.
[16] A.E. Karataş, Ö.L. Gülder, Prog. Energy Combust. Sci. 38 (6) (2012) 818–845.
[17] P.H. Joo, M.R.J. Charest, C.P.T. Groth, L. Ö.Gülder, Combust. Flame 160 (10) (2013) 1990–1998.
[18] L. Figura, A. Gomez, Combust. Flame 161 (6) (2014) 1587–1603.
[19] A. Matynia, J. Molet, C. Roche, M. Idir, S. de Persis, L. Pillier, Combust. Flame 159 (2012) 3300–3311.
[20] A.A. Paletskii, L.V. Kuibida, T.A. Bolshova, O.P. Korobeinichev, R.M. Fristrom, Combust Explos. Shock Waves 32 (3) (1996) 245–250.
[21] Z.Y. Zhou, Y. Wang, X.F. Tang, W.H. Wu, F. Qi, Rev. Sci. Instrum. 84 (2013) 014101.
[22] R.J. Kee, J.F. Grcar, M.D. Smooke, J.A.Miller, Premix: A Fortran program for modelling stedy laminar one-dimensional premixed flames, Sandia National Lab. Report 1992, N SAND85-8240.
[23] W.K. Metcalfe, S.M. Burke, S.S. Ahmed, H.J. Curran, Intl. J. Chem. Kinetics 45 (2013) 638–675 available at http://www.nuigalway.ie/c3/Mechanism_release/frontmatter.html .
[24] A.G. Shmakov, O.P. Korobeinichev, I.V. Rybitskaya, A.A. Chernov, D.A. Knyazkov, T.A. Bolshova, A.A. Konnov, Combust. Flame 157 (2010) 556–565.
[25] O.P. Korobeinichev, V.M. Shvartsberg, A.G. Shmakov, D.A. Knyazkov, I.V. Rybitskaya, Proc. Combust. Inst. 31 (2007) 2741–2748.
[26] C.R. Shaddix, Correcting thermocouple measurements for radiation loss: a critical review, in: Proceedings of the 33rd National Heat Transfer Conference, Paper HTD99-282, Albuquerque, New Mexico, 1999.
[27] T.A. Cool, K. Nakajima, K.A. Taatjes, A. Mcllroy, P.R. Westmoreland, M.E. Law, A. Morel, Proc. Combust. Inst. 30 (2005) 1681–1688.
[28] Y.-K. Kim, K.K. Irikura, M.E. Rudd, M.A. Ali, P.M. Stone, J. Chang, J.S. Coursey, R.A. Dragoset, A.R. Kishore, K.J. Olsen, A.M. Sansonetti, G.G. Wiersma, D.S. Zucker, M.A. Zucker, http://physics.nist.gov/PhysRefData/Ionization.
[29] J. Warnatz, Combust. Sci. Technol. 26 (5) (1981) 203–213.
[30] L. Deng, A. Kempf, O. Hasemann, O.P. Korobeinichev, I. Wlokas, Combust. Flame 162 (5) (2015) 1737–1747.
[31] http://c3.nuigalway.ie/Mechanism_release/validation.html
[32] T.J. Held, F.L. Dryer, Int. J. Chem. Kinet. 30 (11) (1998) 805–830.
[33] F.A Lammers, L.P.H de Goey, Combust. Flame 136 (4) (2004) 533–547.
[34] M.P. Burke, M. Chaos, F.L. Dryer, Y. Ju, Combust. Flame 157 (2010) 618–631.
[35] M.P. Burke, F.L. Dryer, Y. Ju, Proc. Combust. Inst. 33 (2011) 905–912.
[36] R. Kailasanathan, L. Yelverton, T. Fang, W. Roberts, Combust. Flame 160 (2013) 656–670.